REPORT DOCUMENTATION PAGE

Form Approved
OBM No. 0704-0188

AD-A267 642

2. Report Date.	3. Report Type and Dates Covered.
	Final - Journal Article

4. Title and Subtitle.
Acoustical Boundary Location through Texture Analysis of Multibeam Bathymetric Sonar Data

5. Funding Numbers.

Program Element No.	0602435N
Project No.	3585
Task No.	MOG
Accession No.	DN255031
Work Unit No.	113512D

6. Author(s).
Herb Barad*, Andrew B. Martinez*, Brian S. Bourgeois, and Edit J. Kaminsky**

7. Performing Organization Name(s) and Address(es).
Naval Research Laboratory
Marine Geosciences Division
Stennis Space Center, MS 39529-5004

8. Performing Organization Report Number.
JA 351:100:92

9. Sponsoring/Monitoring Agency Name(s) and Address(es).
Naval Research Laboratory
Exploratory Development Program Group
Stennis Space Center, MS 39529-5004

10. Sponsoring/Monitoring Agency Report Number.
JA 351:100:92

11. Supplementary Notes.
Published in MTS Journal.
*Tulane Univ., New Orleans, LA, **Sverdrup Technology, Stennis Space Center, MS

12a. Distribution/Availability Statement.
Approved for public release; distribution is unlimited.

12b. Distribution Code.

DTIC ELECTE AUG 06 1993 S A D

13. Abstract *(Maximum 200 words).*

Texture analysis is performed on multibeam sonar signal returns discriminated angularly by beamforming. A collection of fourteen texture features are computed via co-occurrence matrices and data reduction is then performed using a principal components transformation. Acoustical boundaries (boundaries between regions with homogeneous acoustical properties) are evident from the features. Results indicate that seafloor bottom characteristics can be extracted from these texture features.

93-17935

14. Subject Terms.
Hydrography, bathymetry, optical properties, remote sensing, reverberation

15. Number of Pages.
7

16. Price Code.

17. Security Classification of Report.	18. Security Classification of This Page.	19. Security Classification of Abstract.	20. Limitation of Abstract.
Unclassified	Unclassified	Unclassified	SAR

93 8 4 193

DISCLAIMER NOTICE

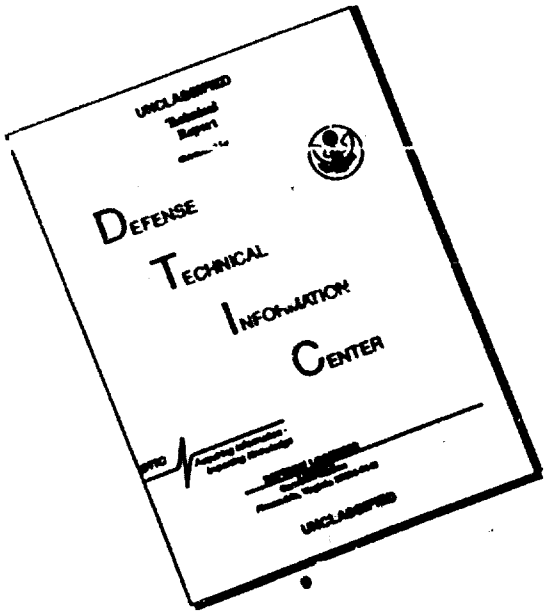

THIS DOCUMENT IS BEST QUALITY AVAILABLE. THE COPY FURNISHED TO DTIC CONTAINED A SIGNIFICANT NUMBER OF PAGES WHICH DO NOT REPRODUCE LEGIBLY.

PAPER

Acoustical Boundary Location through Texture Analysis of Multibeam Bathymetric Sonar Data

Herb Barad
Tulane University
New Orleans, Louisiana

Andrew B. Martinez
Tulane University
New Orleans, Louisiana

Brian S. Bourgeois
Naval Research Lab
Stennis Space Center, Mississippi

Edit J. Kaminsky
Sverdrup Technology
Stennis Space Center, Mississippi

ABSTRACT

Texture analysis is performed on multibeam sonar signal returns discriminated angularly by beamforming. A collection of fourteen texture features are computed via co-occurrence matrices and data reduction is then performed using a principal components transformation. Acoustical boundaries (boundaries between regions with homogeneous acoustical properties) are evident from the features. Results indicate that seafloor bottom characteristics can be extracted from these texture features.

SEAFLOOR IMAGERY FROM MULTIBEAM SONAR DATA

The impetus for generating seafloor acoustic imagery from multibeam sonar data is that more detailed information is available from the returning pulse than is discernible through simple computation of a set of bottom depths (de Moustier, 1986). This is due to the additional information contained in the signal intensity and to the typically high hydrophone sampling rates which provide finer across-track resolution than is possible through beamforming. The resulting imagery displays the response of the seafloor to the acoustic pulse, which is a combination of the local topography as well as the bottom composition. Past efforts have attempted to provide methods for segmenting acoustic imagery into geoacoustic provinces via various image texture processing methods to allow automated classification of the seafloor (Reed IV and Hussong, 1989; Bourgeois and Walker, 1991). However, the process of generating imagery from the raw beamformed data filters at a low-pass rate and distorts the image, and full resolution acoustic imagery is too noisy for successful fine-scale segmentation. In this work analysis is performed on the returning energy, as a function of time, that has been angularly discriminated by beamforming. This approach allows analysis on data that have not suffered the additional generation of noise and introduction of smoothing that occurs when forming an image.

The data used are from the Navy's Sonar Array Survey System (SASS), and complete navigational information is not available; we do not have information as to the actual orientation of the sonar array from ping to ping. Since the data are not fully georeferenced, each ping's swath is processed individually. The results of the texture feature extraction for each ping is then appended, line by line, to form a multiband texture feature set. Parameters used for georeferencing can be used later to find accurate correspondences between seafloor location and bottom characteristics as computed from the texture analysis.

MULTIBEAM DATA PROCESSING

System Hardware

Multibeam bathymetric sonar systems such as SASS, the SeaBeam series, and the EM100 are capable of collecting data which, after proper processing, may be used to accurately map the bottom of the ocean. It is possible to obtain both bathymetry and sidescan-like images from the original raw data. Information about texture of the ocean's bottom may also be generated directly from this data.

For the SASS, the sonar energy from the projector array located on the hull of the survey ship impinges on the bottom of the ocean as a narrow beam perpendicular to the ship's heading. The echo from this swath is received by an array of hydrophones mounted athwartships (perpendicular to the projector) under the survey vessel. The beam width depends on the angle of arrival to the bottom and increases with increasing angle. The unsteered beam width is 0.7°; at 45° it is 0.9°.

Data Processing

Processing starts by reading the raw data recorded by SASS during a survey mission. A detailed description of the original data is given by Bourgeois (1991) and one of the complete processing is given by Kaminsky et al. (1992). The beamforming process is done next by performing delay, filtering, and summing operations through the use of Fourier transforms. This yields an array of return intensities—an intensity for each beamformer bin and each sample time—allowing the returning energy to be resolved into angular bins. Each of the K beamformer bins k correspond to a particular steering angle ϕ_k.

The beamformed data then give us a time history of the energy received from the K look directions. This data must be further processed to determine the time corresponding to the center of the beam, t_c. The peak of the envelope corresponds to the intersection of the maximum response axis (MRA) of the steered beam

and the area ensonified. Once the time t_c has been determined by one of many methods available (Kaminsky et al., 1993) the bathymetry of the area surveyed can be obtained. That is, exact points (x,y,z) that determine the source's position are obtained from each (ϕ_k, t_c) pair.

The intensity data produced by the beamformer may also be used to produce sidescan-like images that show the backscatter intensity. One method of forming image pixels is by summing the total energy returned at a given sample time. In this way, one port and one starboard pixel are generated for each sampling instant. Due to the beamforming process, the image quality can be improved by discarding the returning energy in directions not associated with the dominant pulse for the given sample time using a spatial/temporal window.

In this paper the energy returned along each beam is examined as a function of time. Specifically, the amplitude variations in the returning pulse for each steered beam are analyzed. These amplitude variations are descriptive of the roughness of the seafloor in the region illuminated by the acoustic pulse. If this region is small enough so that the sediment properties may be considered homogeneous then the amplitude variations, or signal 'texture,' are descriptive primarily of the physical roughness of the seafloor.

Variation in local slope is a large source of ambiguity in acoustic imagery: drastically different backscatter intensities are obtained depending upon the acoustic incident angle, making automated analysis of this form of data extremely difficult. The rest of this paper is devoted to texture feature extraction, manipulation, and its interpretations.

TEXTURE ANALYSIS

Texture is a property of pixel values and their spatial relationships. It is insufficient to describe pixel values without considering their spatial relationships to other pixel values. To quantitatively analyze textures, we must use measures that are not only a function of individual pixel values but also multiple pixel values and their relative spatial positioning.

There has been a lot of work done on the analysis of textures. The methods usually fall into certain categories, for example, co-occurrence statistics (Haralick et al., 1973); power spectrum methods (Lendaris and Stanley, 1970); use of Markov models (Cross and Jain, 1983; Manjunath and Chellappa, 1991); structural analysis (Haralick, 1979); and fractal analysis (Pentland, 1984).

Conners and Harlow compare different texture algorithms and conclude that the co-occurrence methods (which they refer to as the *Spatial Gray Level Dependence Method*) is the most powerful method because of its ability to discriminate among a set of textures (Conners and Harlow, 1980). Mastin et al. used co-occurrence methods for SAR (synthetic aperture radar) imagery of water (Mastin et al., 1985). Consequently, we decided to use an analysis based on co-occurrence statistics because of the performance of the method and also the nature of the data acquisition (proper georeferencing information was not available). The data available to the authors do not allow georeferencing or even referencing between pings. Therefore, we only analyze the texture along the one-dimensional path of each ping.

Co-Occurrence Statistics

A histogram is an estimate of the first order statistics of an image (or a region). The normalized histogram is computed as

$$P(i) = \frac{N(i)}{N}, \; i = 0, 1, \ldots 2^b - 1 \qquad (1)$$

where $N(i)$ is the number of pixels in the image (region) with intensity value i, N is the total number of pixels in the image (region), and b is the number of bits per pixel in the image.

The analog to the histogram for second order statistics is the *co-occurrence* matrix. The co-occurrence matrix is also computed in a "census" fashion by counting pairs of occurrences of pixels values given a certain spatial relationship for the pair. The normalized co-occurrence statistics are computed as

$$P(i_1, i_2, d, \theta) = \frac{N(x_1, x_2)}{N}, |x_1 - x_2| = D(d, \theta) \qquad (2)$$

for pairs of pixels at locations x_1 and x_2 having values i_1 and i_2, respectively. The distance measure $D(d,\theta)$ states that the spatial relationship of the pair of pixels is that they are located at a distance magnitude d apart and at an angle θ (or $\theta+\pi$) from each other.

A complete set of co-occurrence statistics would cover all values of d and θ over a meaningful range. The values for θ would vary between 0 and π using some number of discrete steps. The values for d would range from *1* up to some distance where the correlation between pixels is still significant.

In practice, several co-occurrence matrices are computed for several pairs of (d,θ). Figure 1 shows several computed co-occurrence matrices for a simple example 2 bit/pixel image.

One of the disadvantages of the method of co-occurrence matrices is the potentially large amount of data computed for different pairs of d and θ. Only four of the many possible co-occurrence matrices are computed in Figure 1. However, co-occurrence statistics are powerful

FIGURE 1. Sample co-occurrence calculations (Haralick and Shapiro, 1992).

0	0	1	1
0	0	1	1
0	2	2	2
2	2	3	3

		Gray Level			
		0	1	2	3
Gray Level	0	#(0,0)	#(0,1)	#(0,2)	#(0,3)
	1	#(1,0)	#(1,1)	#(1,2)	#(1,3)
	2	#(2,0)	#(2,1)	#(2,2)	#(2,3)
	3	#(3,0)	#(3,1)	#(3,2)	#(3,3)

$$P_{(\theta=0°,d=1)} = \frac{1}{16}\begin{pmatrix} 4 & 2 & 1 & 0 \\ 2 & 4 & 0 & 0 \\ 1 & 0 & 6 & 1 \\ 0 & 1 & 1 & 2 \end{pmatrix} \qquad P_{(\theta=90°,d=1)} = \frac{1}{16}\begin{pmatrix} 6 & 0 & 2 & 0 \\ 0 & 4 & 2 & 0 \\ 2 & 2 & 2 & 2 \\ 0 & 0 & 2 & 0 \end{pmatrix}$$

$$P_{(\theta=135°,d=1)} = \frac{1}{16}\begin{pmatrix} 2 & 1 & 3 & 0 \\ 1 & 2 & 1 & 0 \\ 3 & 1 & 0 & 2 \\ 0 & 0 & 2 & 0 \end{pmatrix} \qquad P_{(\theta=45°,d=1)} = \frac{1}{16}\begin{pmatrix} 4 & 1 & 0 & 0 \\ 1 & 2 & 2 & 0 \\ 0 & 2 & 4 & 1 \\ 0 & 0 & 1 & 0 \end{pmatrix}$$

in that they are invariant to monotonic intensity transformations (Haralick and Shapiro, 1992).

Texture Features

Texture features can then be computed from the co-occurrence matrices. Ballard and Brown (1982) suggest a set of five features, but a more comprehensive set of 14 features is given by Haralick et al. (1973). It is often not clear how these features relate to observable phenomena. However, they have been demonstrated to be useful in classifying images. Using the co-occurrence statistics, these 14 features are computed for each beamformer bin. In this application, only a co-occurrence matrix for $d=1$ and $\theta=0$ is computed. We keep $\theta=0$ since the pings are not georeferenced. The distance d is kept small since we expect the primitives to be relatively small. However, we can still compute more sets of these features for various values of d, but $d=1$ for initial results.

We will follow the notation used in Haralick et al. (1973):

- $p(i, j)$ is the $(i, j)^{th}$ entry in the normalized co-occurrence matrix,
- $p_x(i)$ is the i^{th} entry in the marginal-probability matrix obtained by summing the rows of co-occurrence matrix,
- N_g is the number of gray levels in the image,
- $p_y(j) = \sum_{i=1}^{N_g} p(i,j)$,
- $p_{x+y}(k) = \sum_{i=1}^{N_g} \sum_{j=1}^{N_g} p(i,j)$, $k = i+j = 2, 3, \cdots, 2N_g$,
- $p_{x-y}(k) = \sum_{i=1}^{N_g} \sum_{j=1}^{N_g} p(i,j)$, $k = |i-j| = 0, 1, \ldots, N_g - 1$.
- ϵ is a small constant to prevent taking the log of zero.

The features computed are as follows:

1. angular second moment: a measure of homogeneity of the image,

$$f_1 = \sum_{i=1}^{N_g} \sum_{j=1}^{N_g} \{p(i,j)\}^2. \tag{3}$$

2. contrast: a measure of the contrast or the amount of local variations present,

$$f_2 = \sum_{n=0}^{N_g-1} n^2 \Big\{ \sum_{i=1}^{N_g} \sum_{j=1}^{N_g} p(i,j) \Big\}. \tag{4}$$

3. correlation: a measure of intensity linear dependencies in the image,

$$f_3 = \frac{\sum_{i=1}^{\cdot\cdot} \sum_{j=1}^{N_g} (ij) p(i,j) \quad \mu_x \mu_y}{\sigma_x \sigma_y} \tag{5}$$

where μ_x, μ_y, σ_x and σ_y are the means and standard deviations of p_x and p_y.

4. sum of squares variance: a measure of the variation in the image,

$$f_4 = \sum_{i=1}^{N_g} \sum_{j=1}^{N_g} (i - \mu^2) p(i,j). \quad (6)$$

5. inverse difference moment:

$$f_5 = \sum_{i=1}^{N_g} \sum_{j=1}^{N_g} \frac{1}{1 + (i-j)^2} p(i,j). \quad (7)$$

6. sum average:

$$f_6 = \sum_{i=2}^{2N_g} i p_{x+y}(i). \quad (8)$$

7. sum variance:

$$f_7 = \sum_{i=2}^{2N_g} (i - f_8)^2 p_{x+y}(i). \quad (9)$$

8. sum entropy:

$$f_8 = -\sum_{i=2}^{2N_g} p_{x+y}(i) \log \{p_{x+y}(i) + \epsilon\}. \quad (10)$$

9. entropy:

$$f_9 = -\sum_{i=1}^{N_g} \sum_{j=1}^{N_g} p(i,j) \log\{p(i,j) + \epsilon\}. \quad (11)$$

10. difference variance:

$$f_{10} = \text{variance of } p_{x-y}. \quad (12)$$

11. difference entropy:

$$f_{11} = -\sum_{i=0}^{N_g-1} p_{x-y}(i) \log\{p_{x-y}(i) + \epsilon\}. \quad (13)$$

12. information measure of correlation 1: for this and the next feature, HX and HY are the entropies of p_x and p_y, respectively and

$$HXY = -\sum_{i=1}^{N_g} \sum_{j=1}^{N_g} p(i,j) \log(p(i,j) + \epsilon),$$

$$HXY1 = -\sum_{i=1}^{N_g} \sum_{j=1}^{N_g} p(i,j) \log\{p_x(i)p_y(j) + \epsilon\}, \text{ and}$$

$$HXY2 = -\sum_{i=1}^{N_g} \sum_{j=1}^{N_g} p_x(i)p_y(j) \log\{p_x(i)p_y(j) + \epsilon\}.$$

$$f_{12} = \frac{HYX - HYX1}{\max\{HX, HY\}}. \quad (14)$$

13. information measure of correlation 2:

$$f_{13} = (1 - \exp[-2.0(HXY2 - HXY)])^{1/2}. \quad (15)$$

14. maximum correlation coefficient:

$$f_{14} = (\text{Second largest eigenvalue of } Q)^{1/2}, \quad (16)$$

where,

$$Q(i,j) = \sum_k \frac{p(i,j)p(j,k)}{p_x(i)p_y(k)}$$

These features are computed for each ping along all 256 bins. Actual processing leaves off approximately 30 bins on each end since these represent "near horizontal" directions that produce no useful return information and are mostly noise. Also bins with "dropouts" have been discarded. We know that some pings are missing and that the ones we have are not necessarily parallel to each other. Due to lack of positioning data, we display pings (rows in the image) as if they were parallel to one another. Thus, the features computed for each ping are appended to one another forming 14 "texture feature images" that form the multidimensional feature set.

DATA REDUCTION

It is difficult to interpret large data sets. Therefore, if we can reduce the amount of output to the essentially "useful part" of the data, the reduction will make it easier to manipulate the data and interpret it.

Data reduction is also performed on the multibeam bathymetric data itself (Kaminsky et al., 1992). However, in this case we are concerned with the reduction of the output from the texture analysis.

We have a fourteen-dimensional feature set that was produced from the texture analysis. We cannot just indiscriminately throw away some of the texture features since we do not know which ones will be useful in the characterization of the seafloor bottom. In order to pull out only the most useful features, we need to find the principal components of the feature space. This will give us a feature space where each of the new "features" are decorrelated. Also, the importance of each new feature basically corresponds to the relative size of its associated eigenvalue. So, we now also have a way of distinguishing those components with the greatest information content.

Principal Components

The feature space is currently fourteen-dimensional. We can reduce the dimensionality of the feature space significantly by first transforming the data into a new feature space (still of the same dimensionality). This new feature space should be one in which the data between the features is uncorrelated and also one in which most of the "useful information" is contained in just a few of those features. The Hotelling transform (the discrete formulation of the Karhunen-Loève transform) is used in this case to achieve the *principal components* of the feature space. Unlike many other transformations, the Hotelling transform is data dependent.

The Hotelling transform is computed as follows (Gonzalez and Woods, 1992): Consider a

multispectral image consisting of n bands of size $N \times N$. We form the column vector

$$\mathbf{x} = [x_1 x_2 \ldots x_n]' \tag{17}$$

for each pixel in the image. Therefore, each location in the image is a vector $\mathbf{x}$ consisting of the n pixel values from each of the n bands at that particular location. There are N^2 such vectors in the multispectral image. The mean vector and covariance matrix of $\mathbf{x}$ are defined as

$$\mathbf{m}_x = E\{\mathbf{x}\} \tag{18}$$

and

$$\mathbf{C}_x = E\{(\mathbf{x} - \mathbf{m}_x)(\mathbf{x} - \mathbf{m}_x)'\}. \tag{19}$$

We can estimate both of these statistics using

$$\hat{\mathbf{m}}_x = \frac{1}{N^2}\sum_{k=1}^{N^2}\mathbf{x}_k \tag{20}$$

and

$$\hat{\mathbf{C}}_x = \frac{1}{N^2}\sum_{k=1}^{N^2}\mathbf{x}_k\mathbf{x}'_k - \mathbf{m}_x\mathbf{m}_x'. \tag{21}$$

Once we have calculated these statistics from the multispectral data, we compute the Hotelling transform using the equation

$$\mathbf{y} = \mathbf{A}(\mathbf{x} - \mathbf{m}_x) \tag{22}$$

where $\mathbf{A}$ is the matrix formed from a sorted set of eigenvectors of the covariance matrix $\mathbf{C}_x$. From this we see two important properties:

1. the transformed data $\mathbf{y}$ has zero mean. That is,

$$\mathbf{m}_y = E\{\mathbf{y}\} = 0 \tag{23}$$

2. and that the data are decorrelated

$$\mathbf{C}y = E\{(\mathbf{y} - \mathbf{m}_y)(\mathbf{y} - \mathbf{m}_y)'\} = \mathbf{A}\mathbf{C}_x\mathbf{A}' \tag{24}$$

which is a diagonal matrix. The matrix $\mathbf{A}$ is composed of the eigenvectors of $\mathbf{C}_x$ and it will thus diagonalize it. Therefore, the diagonal elements of the covariance matrix of the transformed data are nothing more than the set of eigenvalues:

$$\mathbf{C}_y = \begin{bmatrix} \lambda_1 & & & & \\ & \lambda_2 & & & \\ & & \lambda_3 & & \\ & & & \ddots & \\ & & & & \lambda_n \end{bmatrix} \tag{25}$$

Assuming that the eigenvalues are sorted from highest to lowest (and the matrix of eigenvectors is correspondingly sorted), then the set of principal components as given in (22) will be sorted so that the first component is the component with the highest variance, the second component is the component with the second highest variance, and so on. We can reconstruct the original set of vectors $\mathbf{x}$ using

$$\mathbf{x} = \mathbf{A}^{-1}\mathbf{y} + \mathbf{m}_x = \mathbf{A}'\mathbf{y} + \mathbf{m}_x. \tag{26}$$

We note that $\mathbf{A}^{-1} = \mathbf{A}'$ since the matrix is orthonormal. In any case, suppose we decide that the principal components associated with the lowest eigenvalues were of little use. This is often true since the magnitude of the smaller eigenvalues are negligible when compared with the others. Therefore, the images associated with these lowest eigenvalues have relatively small variance, that is, there is relatively little useful information contained in these components. We can reduce the dimensionality of the feature space by discarding these components. Suppose we want to keep K of the n components, thus reducing our feature space to only K-dimensional instead of n-dimensional. We can do this by forming a matrix $\mathbf{A}_K$ composed of the K eigenvectors corresponding to the K largest eigenvalues. We can alter (26) to form approximations of the original data as

$$\hat{\mathbf{x}} = \mathbf{A}'_K\mathbf{y} + \mathbf{m}_x. \tag{27}$$

The mean square error between $\mathbf{x}$ and $\hat{\mathbf{x}}$ is

$$e_{ms} = \sum_{j=1}^{n}\lambda_j - \sum_{j=1}^{K}\lambda_j. \tag{28}$$

The Hotelling transform is optimal for minimizing the quantity e_{ms} (Gonzalez and Woods, 1992).

For the purposes of feature extraction, we can loosely interpret this method as a means to

1. find a new set of features (the principal components), such that these features are decorrelated and have a "measure of relative importance" associated with them, and
2. reduce the dimensionality of the feature space providing data compression.

RESULTS

Figures 2 through 5 show the first four principal components. The contrast has been improved so that the characteristics of the features are more visible. The horizontal band across the center of each feature corresponds to the nadir and near-nadir (almost vertical) beam steering angles. This band represents a uniform texture which is expected for this region since, at high incident angles, the acoustic return is largely due to specular reflection instead of backscatter. The returning pulse will typically be relatively smooth for high angles, and a texture measure of this sort will not reveal interesting

FIGURE 2. First principal component.

FIGURE 3. Second principal component.

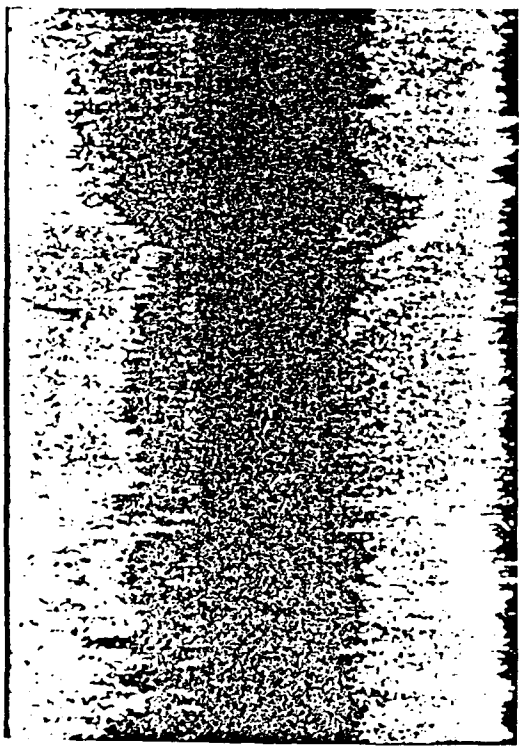

FIGURE 4. Third principal component.

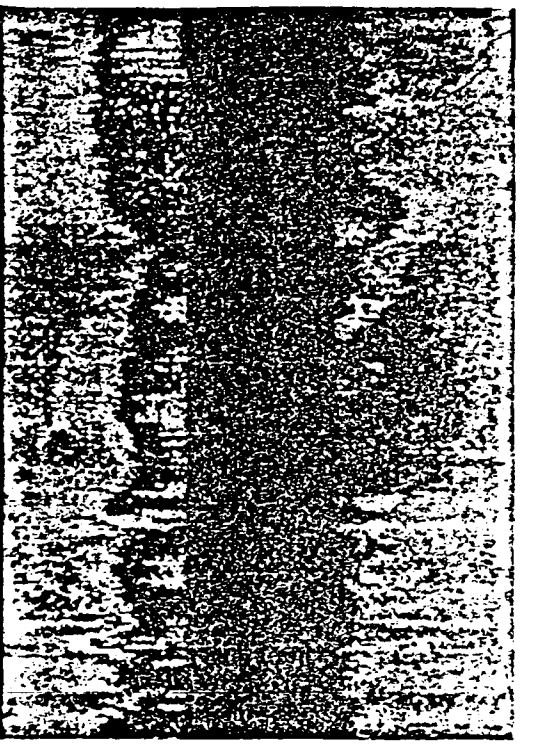

FIGURE 5. Fourth principal component.

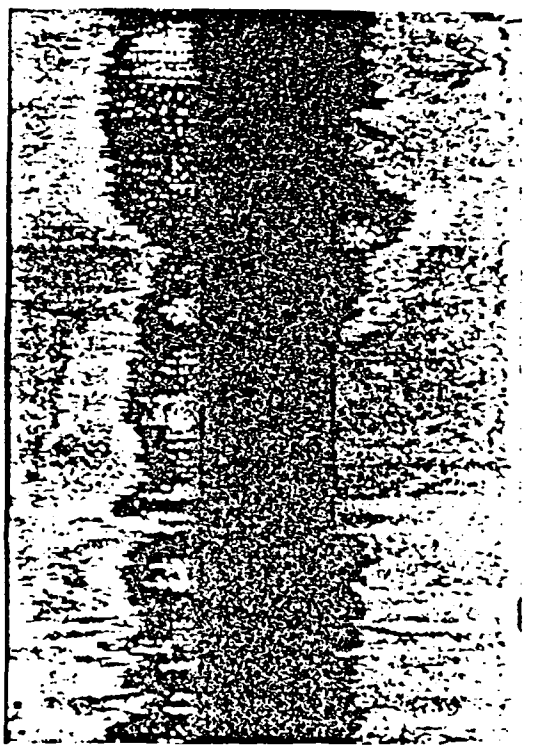

features until the acoustic return is predominately non-specular.

It is evident from these features that there are regions with similar texture characteristics. The texture is computed from the backscatter returns and represents spatial relationships of the way in which the backscatter varies along the pings. Thus, regions with similar features represent regions of similar acoustical backscattering properties. The acoustical

boundaries are the locations of significant transition between acoustical properties.

Figure 6 (see the outside back cover of this issue) shows the first principal component (the one with the most variance) mapped to a terrain obtained from the bathymetric data. The center band running through the middle represents the nadir and near-nadir positions as explained earlier.

CONCLUSION

The texture analysis provides a description of the directional backscatter returns using second order statistical properties and is a useful measure. This is especially useful even for non-calibrated systems. Regions of homogeneous acoustical properties are brought out through this texture analysis. Variations in backscatter are due to changes in bottom types, surface orientation, and roughness. Due to the method used in this analysis the effect of orientation is reduced and, assuming a small enough acoustic footprint, the bottom type may be considered homogeneous. Thus these texture measures provide an indication of micro-roughness (i.e., the small-scale surface roughness that exists below the resolution of the resolvable bathymetry).

Clearly, proper georeferencing information would improve the results so that a more accurate classification of the acoustical properties and the corresponding bottom location would result. Thus, the texture analysis contributes and plays an important role in seafloor bottom classification and mapping. In addition, work is currently being performed at Tulane University and the Naval Research Laboratory to classify the acoustical properties using neural models trained by the texture features.

ACKNOWLEDGMENTS

The authors acknowledge the Office of Naval Technology, project element 602435N, managed by Dr. Herb Eppert, Naval Research Laboratory, Stennis Space Center, Mississippi. This paper, NRL Contribution Number JA351:100:92, is approved for public release; distribution is unlimited. Drs. Barad and Martinez are also sponsored by National Science Foundation/Louisiana Board of Regents grant NSF/LEQSF(1992-93)-ADP-04.

REFERENCES

Ballard, D.H. and Brown, C.M. 1982. *Computer Vision*. Englewood Cliffs, N.J.: Prentice Hall.

Bourgeois, B.S. 1991. SASS DAT data format. Technical Report, NOARL, Code 351.

Bourgeois, B.S. and Walker, C. 1991. Sidescan Sonar Image Interpretation with Neural Networks. In *Oceans '91 Conference Proceedings*, vol. 3, pp. 1687–1694. New York: Inst. of Electrical and Electronics Eng.

Conners, R. and Harlow, C. 1980. A theoretical comparison of texture algorithms. *IEEE Trans. on Pattern Analysis and Machine Intelligence*, PAMI-2(3):204–222. New York: Inst. of Electrical and Electronics Eng.

Cross, G. and Jain, A. 1983. Markov random field texture models. *IEEE Trans. on Pattern Analysis and Machine Intelligence*, PAMI-5(1):25–39. New York: Inst. of Electrical and Electronics Eng.

de Moustier, C. 1986. Beyond bathymetry: Mapping acoustic backscattering from the deep seafloor with Sea Beam. *Journal of Acoustical Society of America*, 79(2):316–331.

Gonzalez, R.C. and Woods, R.E. 1992. *Digital Image Processing*. Reading, Mass.: Addison-Wesley.

Haralick, R. 1979. Statistical and structural approaches to texture. *Oceans '79 Conference Proceedings*, 67(5):786–804. New York: Inst. of Electrical and Electronics Eng.

Haralick, R., Shanmugam, K. and Dinstein, I. 1973. Textural features for image classification. *IEEE Transactions on Systems, Man, and Cybernetics*, SMC-3(6):610–621. New York: Inst. of Electrical and Electronics Eng.

Haralick, R.M. and Shapiro, L.G. 1992. *Computer and Robot Vision*, vol. 1. Reading, Mass.: Addison-Wesley.

Kaminsky, E.J., Bourgeois, B.S., Martinez, A.B. and Barad, H. 1992. SASS imagery development. Technical Report, NRL, Code 351.

Kaminsky, E.J., Bourgeois, B.S., Zabounidis, C., Capell, W.J. and Martinez, A.B. 1993. Determination of the time of energy return from beamformed data. In *Acoustical Classification and Mapping of the Seabed*, Bath, UK. Underwater Acoustics Group. Submitted for review.

Lendaris, G. and Stanley, G. 1970. Diffraction pattern sampling for automatic pattern recognition. *Oceans '70 Conference Proceedings*, 58:198–216. New York: Inst. of Electrical and Electronics Eng.

Manjunath, B. and Chellappa, R. 1991. Unsupervised texture segmentation using markov random field models. *IEEE Trans. on Pattern Analysis and Machine Intelligence*, 13(5):478–482. New York: Inst. of Electrical and Electronics Eng.

Mastin, G.A., Harlow, C.A., Huh, O.K. and Hsu, S.A. 1985. Methods of obtaining offshore wind direction and sea-state data from x-band aircraft SAR imagery of coastal waters. *IEEE Journal of Oceanic Engineering*, OE-10(2):159–174.

Pentland, A. 1984. Fractal-based description of natural scenes. *IEEE Trans. on Pattern Analysis and Machine Intelligence*, PAMI-6(6):661–674.

Reed IV, T. and Hussong, D. 1989. Quantitative Analysis of SeaMARC II Side-Scan Sonar Imagery. *J. Geophys. Res.*, 94(B6):7469–7494.